Supplementary Information

Tailored Morphology and Highly Enhanced Phonon Transport in Polymer Fibers: A Multiscale Computational Framework

Shangchao Lin[1,*,§], Zhuangli Cai[1,2,§], Yang Wang[2], Lingling Zhao[2], and Chenxi Zhai[3]

[1]Institute of Engineering Thermophysics, School of Mechanical and Power Engineering, Shanghai Jiao Tong University, Shanghai, 200240, China

[2]Key Laboratory of Energy Thermal Conversion and Control of Ministry of Education, School of Energy and Environment, Southeast University, Nanjing, Jiangsu 210096, China

[3]Department of Mechanical Engineering, FAMU-FSU College of Engineering, Florida State University, Tallahassee, Florida 32310, United States

*Corresponding author's contact information:

Shangchao Lin, phone: +86 18862117400; E-mail: shangchaolin@sjtu.edu.cn

[§]These authors contributed equally to this work.

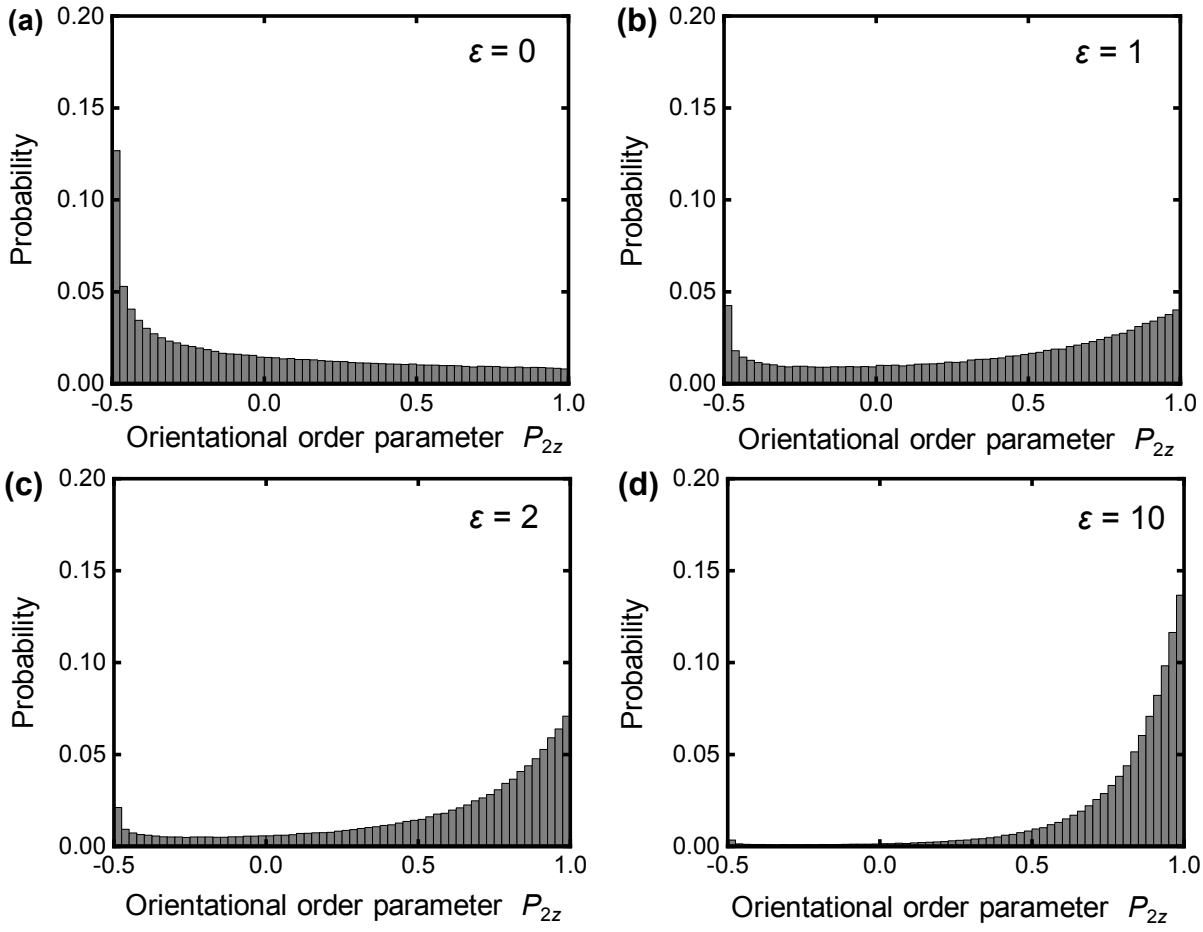

Supplementary Figure 1. The probability distribution of orientational order parameter P_{2z} at strains of 0 (a), 1 (b), 2 (c), and 10 (d) after annealed stress relaxation to 300 K under a fiber drawing temperature of 500 K and a strain rate of 5×10^{7} s^{-1}.

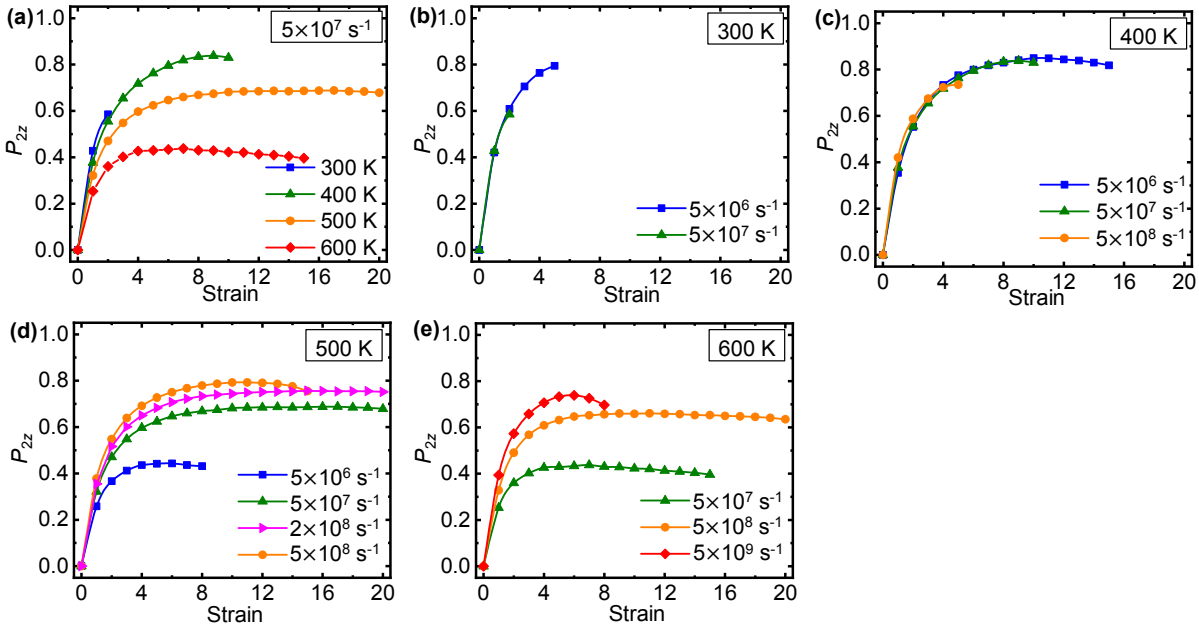

Supplementary Figure 2. The evolutions of orientational order parameter P_{2z} of bulk PE as a function of strain before stress relaxation obtained from (a) various drawing temperatures and a fixed strain rate of 5×10^7 s^{-1} and (b, c, d and e) various strain rates and fixed drawing temperature of 300, 400, 500 and 600 K, respectively.

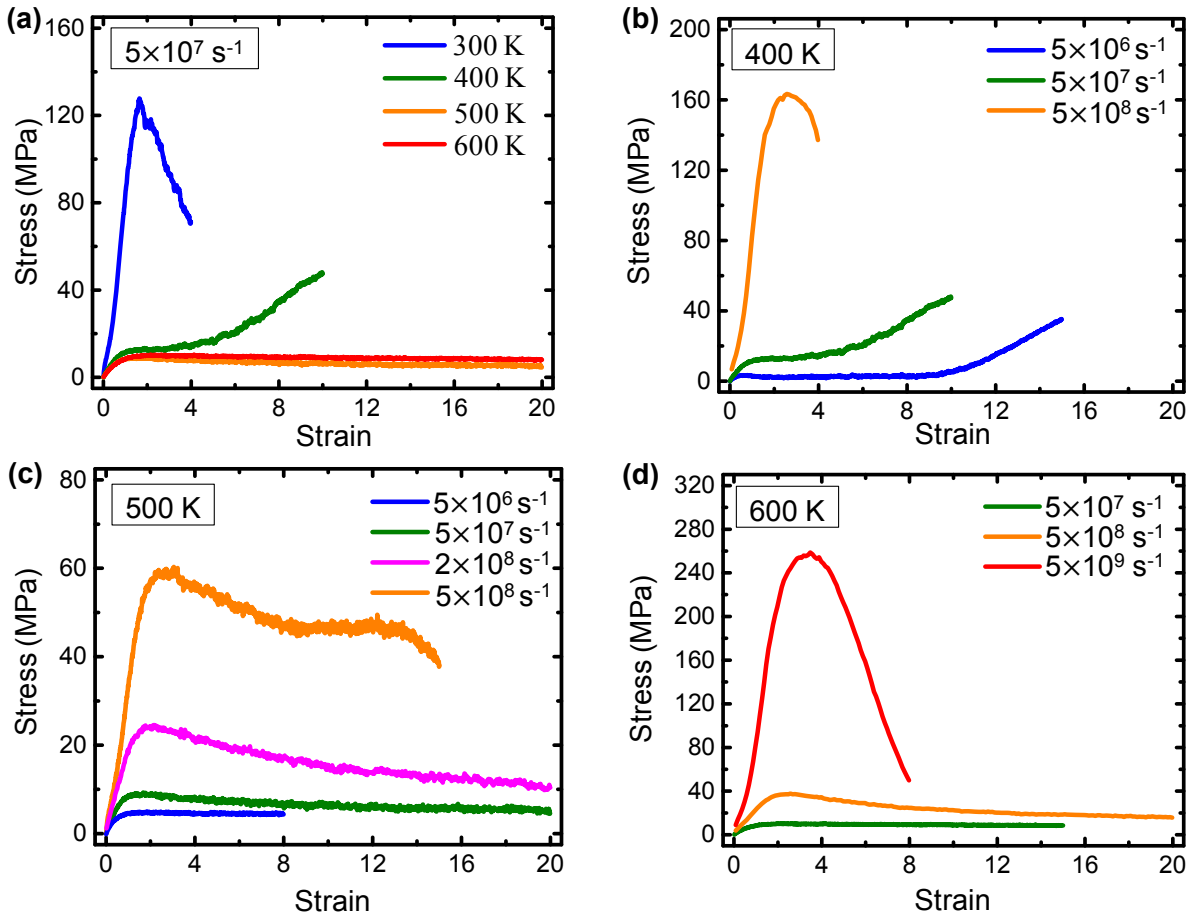

Supplementary Figure 3. Stress-strain responses during the fiber drawing process at (a) a fixed drawing speed (strain rate) of 5×10^{7} s^{-1}, but different drawing temperatures, and (b, c, and d) fixed drawing temperatures of 400, 500, and 600 K, respectively, but different strain rates.

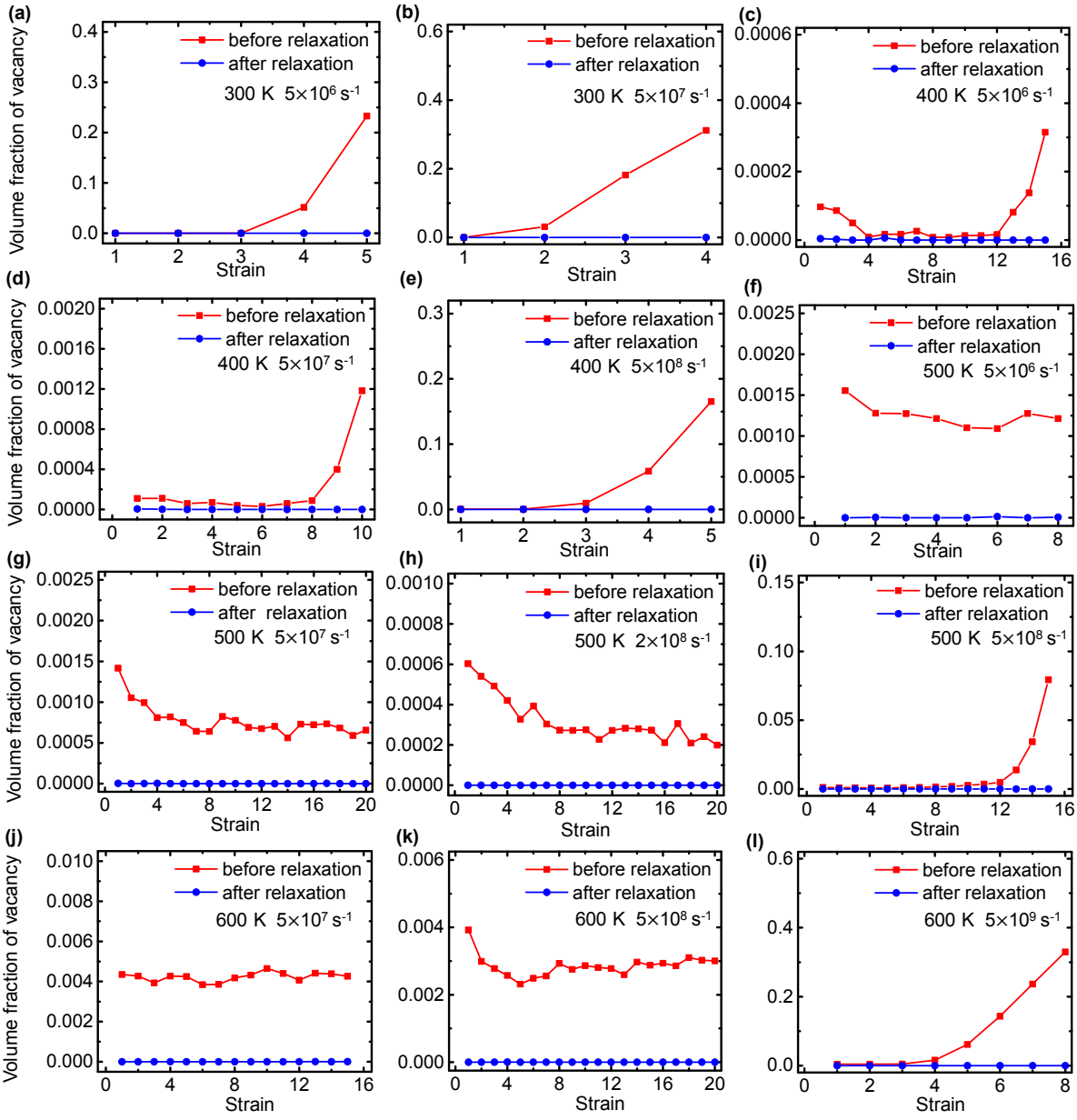

Supplementary Figure 4. Volume fractions of nanovoid vacancies as a function of strain before and after annealed stress relaxation to 300 K under different fiber drawing temperatures and speeds (strain rates). These values were derived by the surface construction algorithm[1] in the program OVITO[2].

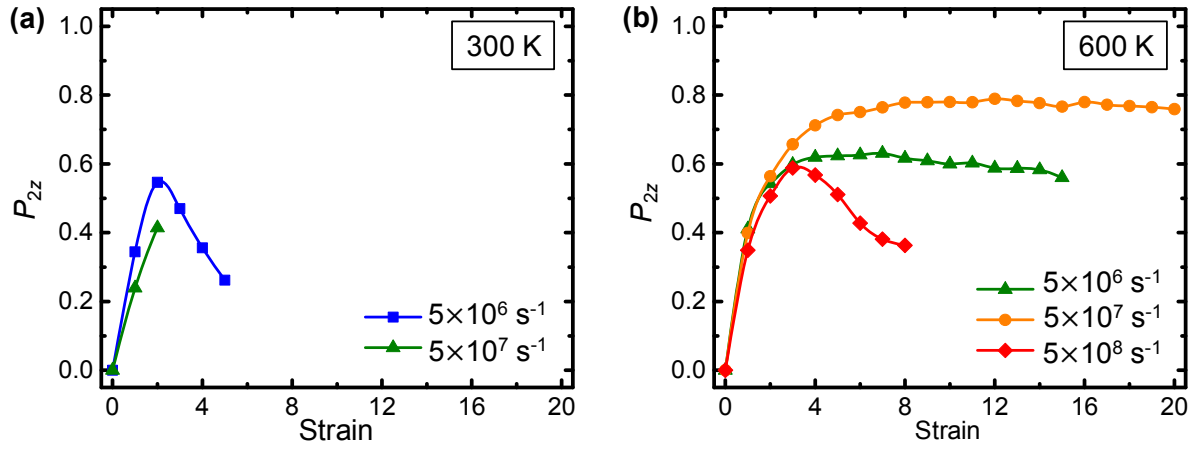

Supplementary Figure 5. The evolutions of orientational order parameter P_{2z} of bulk PE as a function of strain, obtained from different strain rates and two drawing temperatures of (a) 300 K and (b) 600 K.

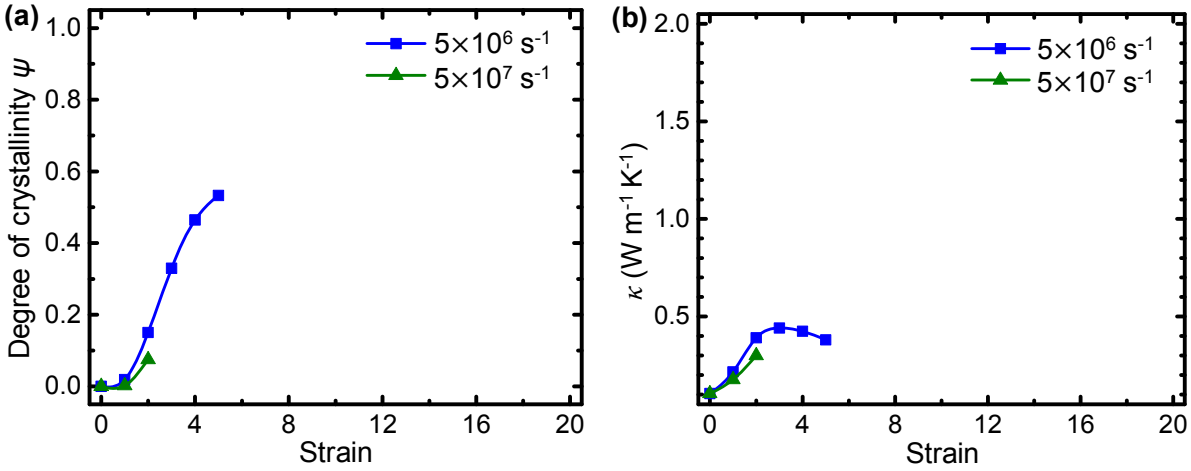

Supplementary Figure 6. (a) Degree of crystallinity and (b) thermal conductivity with increasing the strains under a drawing temperature of 300 K and strain rates of 5×10^6 and 5×10^7 s^{-1}.

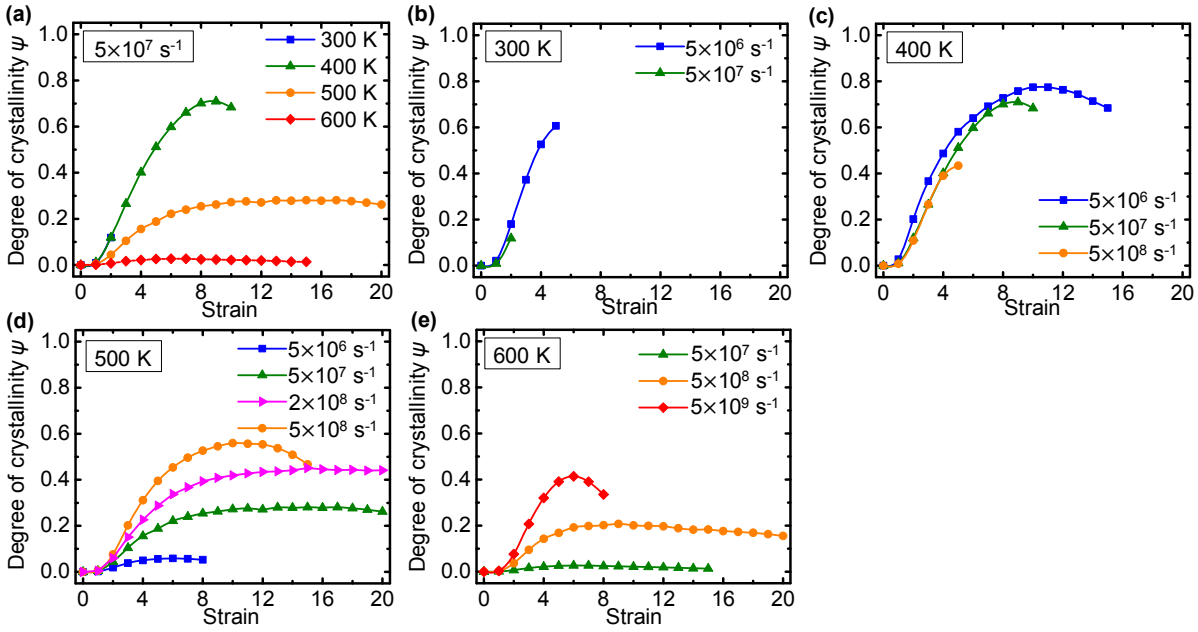

Supplementary Figure 7. The evolutions of degree of crystallinity Ψ of bulk PE as a function of strain before annealed stress relaxation, obtained at (a) a fixed strain rate of 5×10^7 s^{-1}, but different drawing temperatures, and (b, c, d and e) fixed drawing temperatures of 400, 500, and 600 K, respectively, but different strain rates.

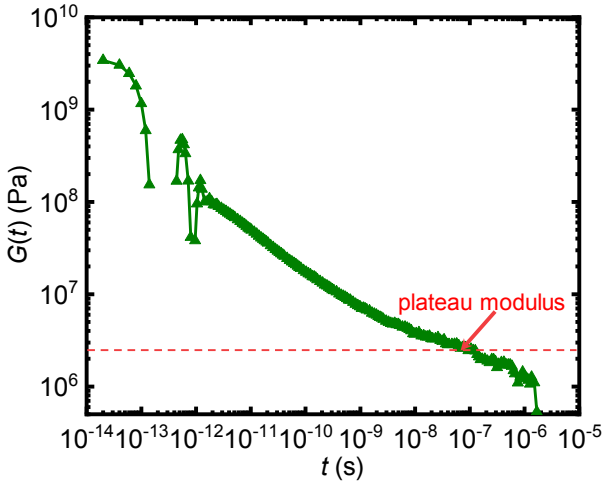

Supplementary Figure 8. Time-evolutions of stress relaxation modulus, $G(t)$, for undrawn amorphous PE at 400 K. The plateau modulus of $G(t)$ at 400 K is estimated to be ~2.5 MPa.

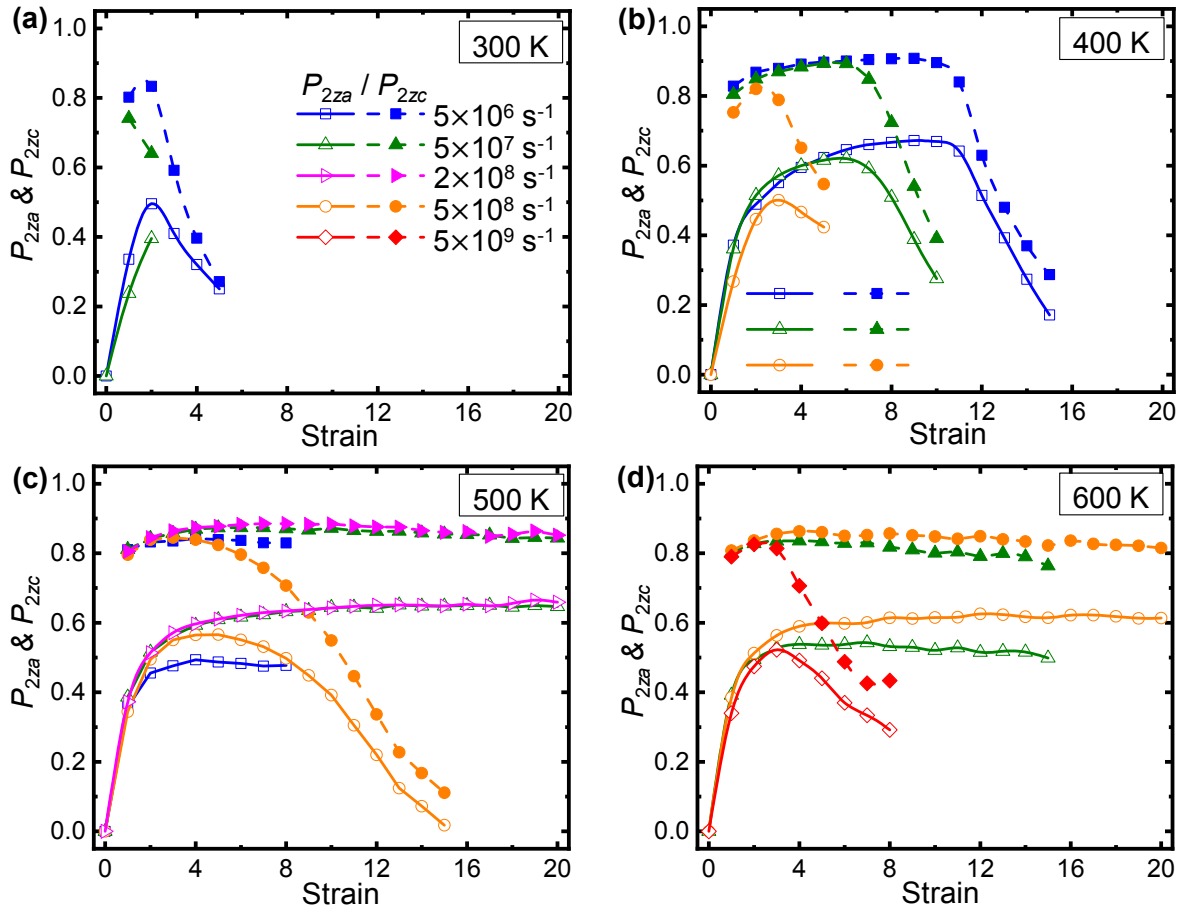

Supplementary Figure 9. The evolutions of orientational order parameter P_{2za} over all amorphous bead and P_{2zc} over all crystalline bead of bulk PE as a function of strain, obtained from different strain rates and fixed drawing temperatures of (a) 300 K, (b) 400 K, (c) 500 K, and (d) 600 K.

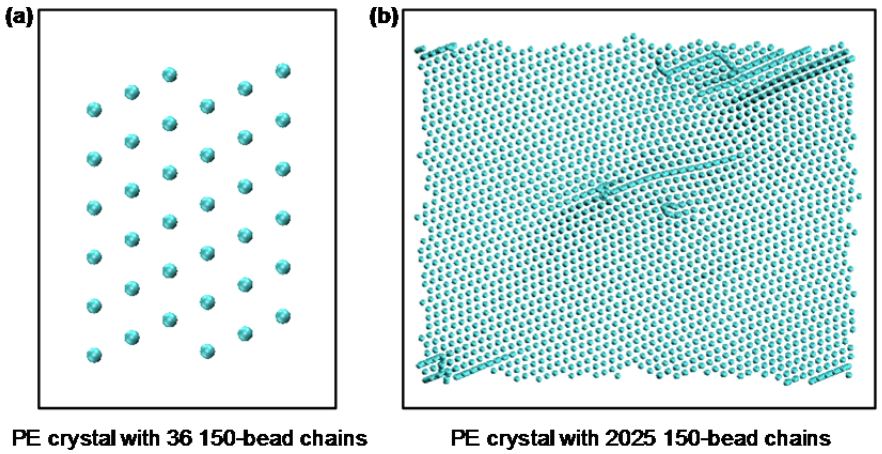

Supplementary Figure 10. Cross-sectional CG-MD simulation snapshots of (a) the optimized PE crystal with 36 perfectly aligned 150-bead chains for calculating the thermal conductivity using the Green-Kubo method, and (b) the optimized PE crystal with 2025 150-bead chains for calculating the phonon VDOS. The snapshot in (a) is zoomed-in by 5 times with respect to (b).

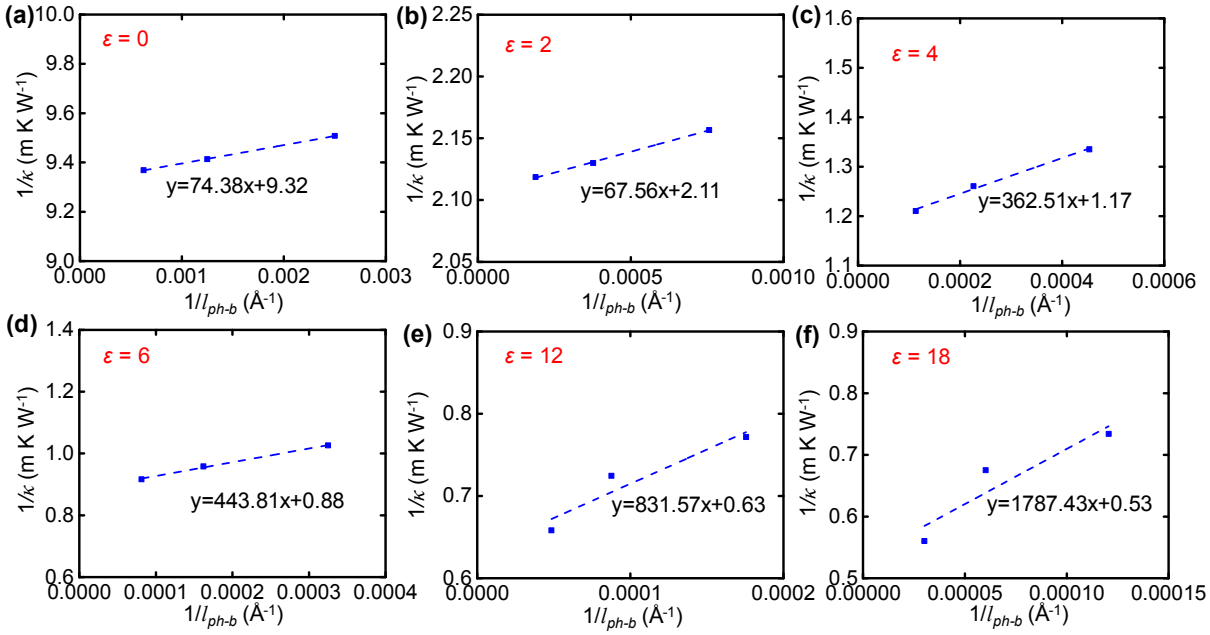

Supplementary Figure 11. $1/\kappa$ of the thermally drawing PE fiber as a function of $1/l_{ph\text{-}b}$ at strain levels ε = 0, 2, 4, 6, 12 and 18, respectively, under a strain rate of 5×10^{7} s^{-1} and a drawing temperature of 500 K.

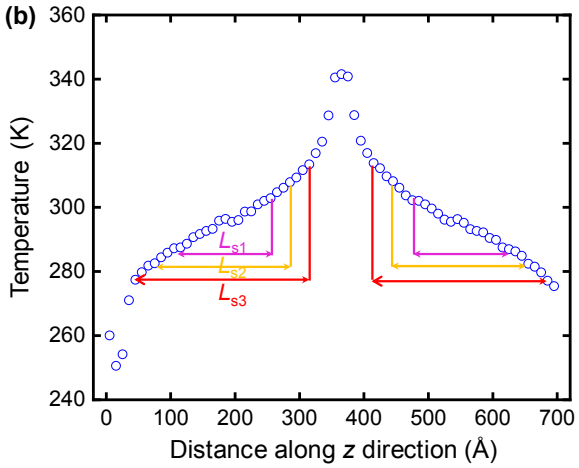

Supplementary Figure 12. Temperature profile of a single 120-bead PE chain obtained from NEMD simulations, where three different linear regions of L_{s1}, L_{s2} and L_{s3} are chosen for linear fitting. The thermal conductivities determined in these three regions are 25.9, 28.2 and 29.8 W m^{-1} K^{-1}, respectively. The resulting standard deviation of 1.9 W m^{-1} K^{-1} is quite small compared to the average.

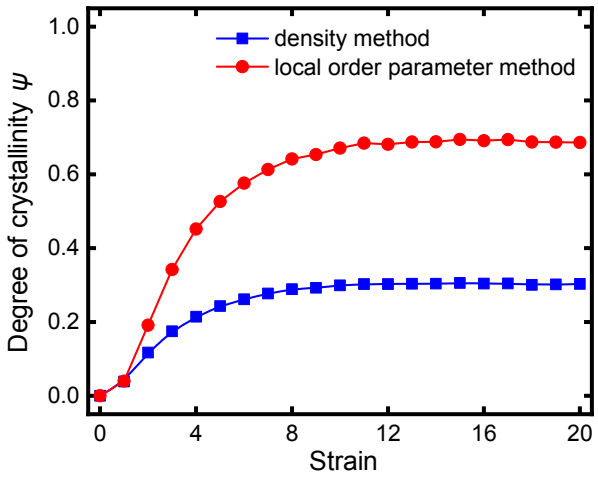

Supplementary Figure 13. Degrees of crystallinity Ψ, determined by the density method for a PE system with an averaged density ρ ($\Psi = \frac{\rho-\rho_0}{\rho_{cry}-\rho_0}$, where ρ_0 and ρ_{cry} are the densities of

amorphous and perfect crystalline PE, respectively) and the local order parameter method (see Eq. 10 in the main text), with increasing strain under a strain rate of 5×10^{7} s^{-1} and a drawing temperature of 500 K.

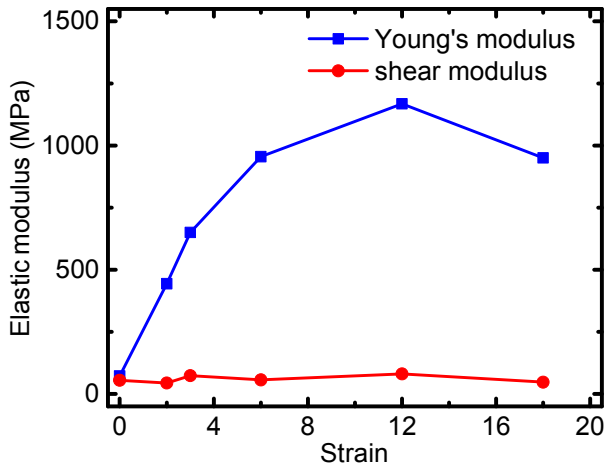

Supplementary Figure 14. Young's and shear moduli of bulk PE with increasing the strain after the annealed stress relaxation to 300 K under a strain rate of 5×10^{7} s^{-1} and a drawing temperature of 500 K.

Supplementary Method: Development of a Predictive Coarse-Grained Force Field

In the CG model, every 5 consecutive methylene groups ($-CH_2-$) are lumped into one bead which sits at the center of mass of the 5 CH_2 groups as shown in **Fig. 1(a)**. Note that lumping 5 ($-CH_2-$) units into one bead not only yields high computational efficiency, but also enables us to reproduce the crystallization process, a key structural feature affecting the thermal conductivity of PE fibers. This is because the equilibrium bond length (location of the peak in the bond length distribution profiles in **Supplementary Fig. 15(a, b)**) for such a bead assignment matches the

diameter of the bead (location of the first radial distribution function peaks in **Supplementary Fig. 18(a, b)**) well, which has been proven a critical criterion to enable polymer crystallization in CG-MD simulations[3]. The CG potential for PE is expressed as:

$$V_{CG} = V_{bond} + V_{angle} + V_{nonbonded} \quad \text{(S1)}$$

which contains the bond stretching, angular bending and nonbonded potentials.

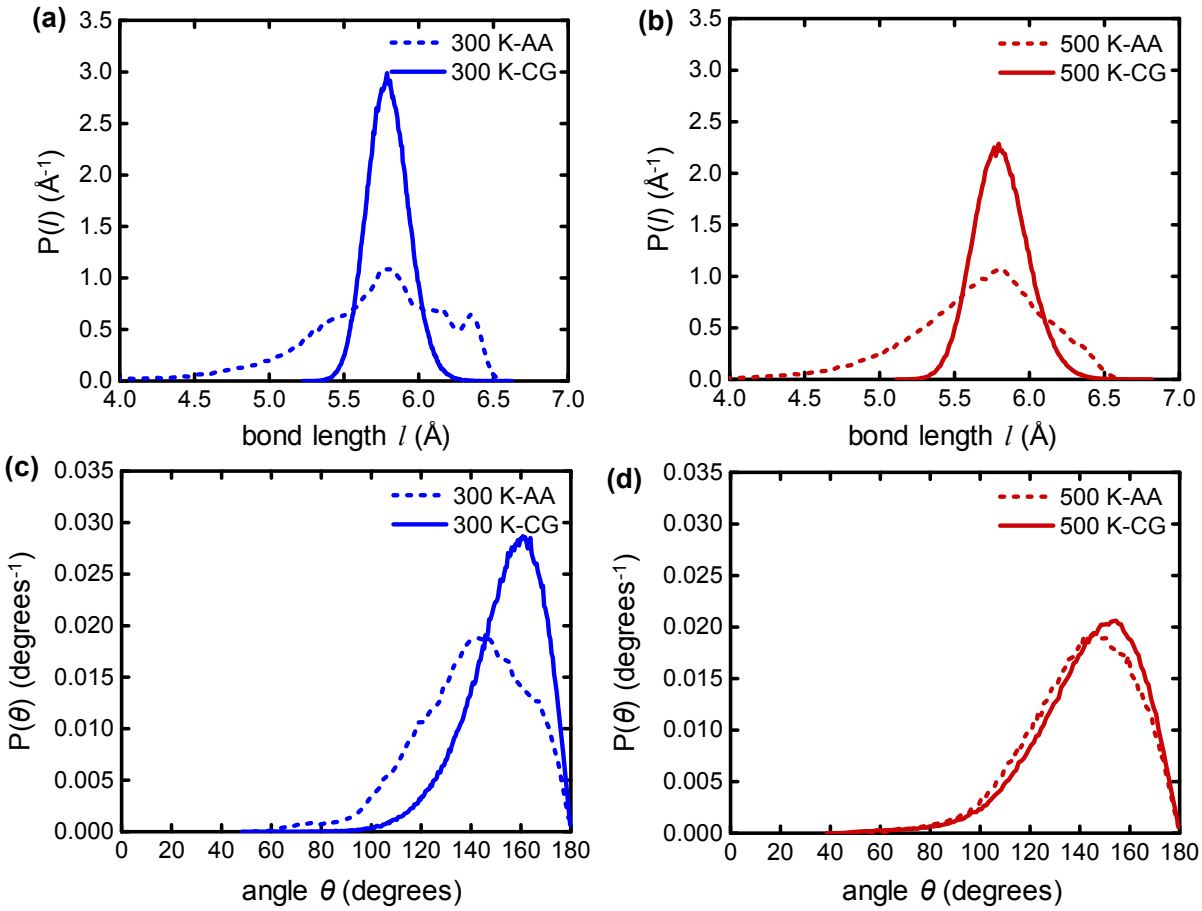

Supplementary Figure 15. Comparison between AA-MD and CG-MD simulations with respect to bond length and angle distributions. (a) and (c) The bond length and angle distributions at 300 K; (b) and (d) The bond length and angle distributions at 500 K.

The parameterization of the CG potential relies on the AA-MD simulations of 400 PE chains, each containing 72 carbon atoms (72-mer). The AA-MD simulations of PE chains are carried out using the AIREBO potential[4]. The AIREBO potential was confirmed to accurately predict the TC of bulk PE single crystal (180±65 W m^{-1} K^{-1}) compared with the experimental value of PE nanofibers (104 W m^{-1} K^{-1})[5] and quantum mechanics calculated value[6] of 160 W m^{-1} K^{-1}. Considering that the PE fibers are thermally drawn above their glass transition temperature and quenched to the room temperature, benchmarking AA-MD simulations of amorphous bulk PE systems were performed with a timestep of 0.5 fs at two representative thermodynamic states: one at 500 K with an experimentally reported density[7] of 0.71 g cm^{-3}, and the other at 300 K with a theoretically predicted density[8,9] of 0.82 g cm^{-3}. Please note that the AIREBO potential slightly underestimates the density of bulk PE under the *NPT* ensemble, and therefore, the AA-MD simulations were run under the *NVT* ensemble to reproduce the experimental amorphous PE densities using the Nosé-Hoover thermostat[10,11]. The initial structure was generated as a bulk PE crystal. The system was first equilibrated for 12 ns at 500 K, after which the polymer units have moved a distance larger than the averaged end-to-end distances of all the chains, indicating that the local conformations have been adequately sampled[12]. The polymer configurations at 500 K were sampled every 0.05 ns over the last 3 ns of the AA-MD simulation. Then the density of the polymer melt was adjusted to 0.82 g cm^{-3} by change the volume of the simulation box. Then the system was sequentially relaxed through instantaneous T coupling at 300 K under the *NVT* ensemble for 5 ns, where the potential energy and pressure values achieve equilibrium within the first 2 ns. The polymer configurations at 300 K were sampled every 0.05 ns over the last 3 ns as

well.

Similar to the AA-MD simulations, CG-MD simulations of 400 14-bead chains, each as a CG representation of the 72-mer AA chain, were performed with a timestep of 20 fs. The initial structure was created as a bulk PE crystal. The system was first equilibrated for 20 ns at 500 K with a density of 0.71 g cm^{-3} under the *NVT* ensemble. The CG configurations at 500 K were sampled every 1 ns over the last 40 ns of the CG-MD simulation. Then the density of the polymer melt was adjusted to 0.82 g cm^{-3} by change the volume of the simulation box. Then the system was sequentially relaxed through instantaneous T coupling at 300 K under the NVT ensemble for 60 ns. The polymer configurations at 300 K were sampled every 1 ns over the last 40 ns as well.

The terms in the CG potential are parameterized following an order based on the relative interactive strengths, from strong to weak[13]:

$$V_{bond} \rightarrow V_{angle} \rightarrow V_{nonbonded} \tag{S2}$$

Generally, distributions of bond length and angles from AA-MD simulations are used as the target properties in the parameterization of CG potentials. The atomistic trajectory in the AA-MD simulation is converted into the CG trajectory according to the above mapping scheme. We chose the Morse potential as the functional form for the bond stretching potential V_{bond}, which can capture the anharmonic feature critical for describing the phonon-phonon scattering. Specifically,

$$V_{bond} = D_b\left[e^{-2\alpha_b(l-l_0)} - 2e^{-\alpha_b(l-l_0)}\right] \tag{S3}$$

where l_0 is the equilibrium bond distance to achieve a minimum potential energy of $-D_b$, and α_b measures the rate of decay of the potential. We chose the dissociation energy, D_b = 84 kcal mol^{-1},

based on the dissociation energy of a single C-C bond[14], and l_0 = 5.8 Å based on the AA-MD simulated distance (the peak position in the probability distribution, see **Supplementary Fig. 15**) between two $(CH_2)_5$ groups.

Since the TC of individual extended polymer chain is critical in reproducing the TC of bulk polymer systems, we determined the parameter α_b by matching the TC of a single chain in the CG model with that in the AA model at 300 K. Note that the bond stretching potential derived by matching the AA-MD bond length distribution is too soft and cannot reproduce the real TC of individual chains. Therefore, the optimized α_b value would lead to a stiffer CG bond stretching potential compared to that in the AA model as shown in **Supplementary Fig. 15**. To keep the aligned-chain state in TC calculations of a single chain, one end of the PE chain is covalently bonded to the other end through the periodic boundary condition. Different chain lengths, including 400, 480, 600, 680 and 800 CH_2 groups in the AA model, which correspond to 80, 96, 120, 136 and 160 beads in the CG model, were considered in non-equilibrium molecular dynamics (NEMD) simulations (the Müller-Plathe method) to calculate TCs, as shown in **Supplementary Fig. 16(a)**.

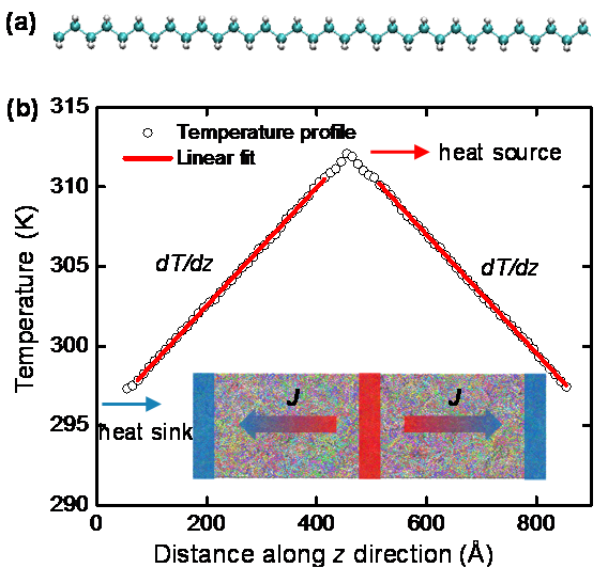

Supplementary Figure 16. (a) Schematic drawing of an extended single PE chain. (b) Equilibrated temperature profile for bulk PE along the z-axis. The inset illustrates the Müller-Plathe algorithm applied on amorphous PE consisting of 2025 150-bead chains for establishing the temperature gradient $\partial T/\partial z$.

In order to reproduce the flexibility of polymer chains and the crystalline structural property of bulk polymers, we obtained the angular bending potential parameter in the CG model by matching the angle distribution with that in AA-MD simulation. We selected the cosine potential, assuming an equilibrium angle of 180°, as the functional form of the angular bending potential V_{angle}, which can realize polymer crystallization in CG-MD simulations[3]. Specifically,

$$V_{angle} = k_a(1 + cos\theta) \tag{S4}$$

where the angular bending force constant k_a = 4 kcal mol^{-1} was determined by matching the angle distribution with that in AA-MD simulation, as shown in **Supplementary Fig. 15**.

To obtain the CG nonbonded potential, we applied the multiscale iterative Boltzmann inversion (MS-IBI) approach. In MS-IBI, the radial distribution functions (RDFs) of the center

of mass of $(CH_2)_5$ groups were first obtained from AA-MD simulations, which are regarded as the target property in the parameterization of nonbonded potential. Note that the bonded nearest and second-nearest neighbors within each chain are excluded in the RDFs. The initial nonbonded potential is assumed to be the Boltzmann inversion of the target RDF, $g^*(r)$, averaged over the two thermodynamic states at 300 and 500 K:

$$V_{nonbonded,0}(r) = -\frac{1}{2}\sum_s k_B T_s \ln[g_s^*(r)] \tag{S5}$$

where k_B is the Boltzmann constant and the subscript "s" represents the various thermodynamic states. The cutoff distance of the nonbonded potential is r_{cutoff} = 12 Å. After running a trial of CG-MD simulations for 60 ns at each state using the numerical-form potential obtained from Eq. 5, the original version of the potential is updated to version *i* iteratively by:

$$V_{nonbonded,i+1} = V_{nonbonded,i} + \frac{1}{2}\sum_s k_B T_s \ln\left[\frac{g_s^i(r)}{g_s^*(r)}\right] \tag{S6}$$

where $g_s^i(r)$ is the RDF of the update potential of version *i*. The convergence of the iteration process can be quantified by evaluating the following merit function:

$$f = \int_0^{r_{cutoff}} e^{-\frac{r}{\sigma}}\left[g^*(r) - g^i(r)\right]^2 dr \tag{S7}$$

where σ is the vdW diameter of the CG bead, which was chose to be 5.8 Å from the location of the first peak in $g^*(r)$. When f is smaller than 0.02 or does not decrease further, the iteration is considered converged and then ended.

Supplementary Discussion: Training and Validation of the Coarse-Grained Force Field

The equilibrium CG bond distance l_0 is determined through the probability distributions of bond length at 300 K and 500 K in AA-MD simulations as shown in **Supplementary Fig. 15(a, b)**. To determine the CG parameter α_b, we adjusted the value of α_b such that the TCs of single PE chains with different lengths predicted using CG-MD simulations match those using AA-MD simulations at 300 K, as shown in **Supplementary Fig. 17**. The distribution of bond length from CG-MD simulation is narrower than that from AA-MD simulation, which is required to reproduce the correct TC values. By adjusting the CG parameter k_a in the angular bending potential, the probability distributions of angles in AA-MD and CG-MD simulations at 500 K match each other reasonably well (**Supplementary Fig. 15(c, d)**), while some differences exist at 300 K probably due to the higher degrees of freedom in AA bulk PE models. Please note that the angular bending potential has a minor impact on the calculated TC compared to the bond stretching potential because the angular bending energy (in the order of 10 kcal mol^{-1}) is significantly lower than the bond stretching energy (in the order of 100 kcal mol^{-1}). Therefore, we can adjust the value of k_a independently after fixing the value of α_b. The same reason applies to the nonbonded terms parameterized below, which can be tuned independently after fixing all the bond and angular terms.

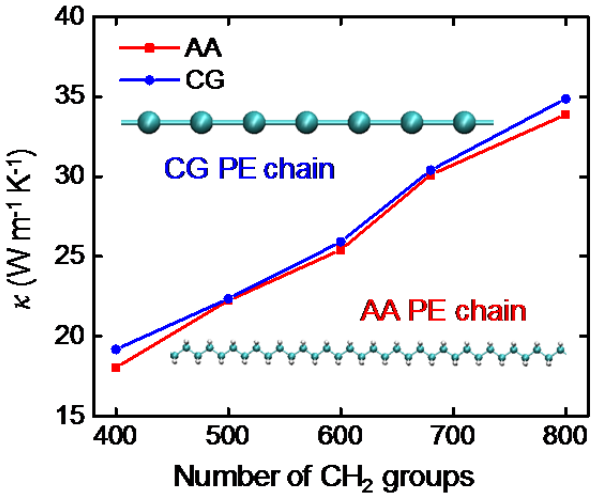

Supplementary Figure 17. The thermal conductivity of extended single PE chains composed of different numbers of CH_2 groups in AA-MD and CG-MD simulations.

To further validate the CG potential, we calculated the end-to-end distance and radius of gyration, as listed in **Supplementary Table 1**. Both end-to-end distance and radius of gyration in CG-MD simulations are slightly larger than those in AA-MD simulation at temperatures of 300 K and 500 K. The deviations between end-to-end distance and radius of gyration in the CG-MD and the AA-MD simulations at 300 K are slightly larger than those at 500 K. This is due to same reason for the slightly larger deviations in the angular distributions between AA-MD and CG-MD simulations at 300 K than those at 500 K.

Supplementary Table 1: Computed end-to-end distance and radius of gyration of PE chain in AA-MD and CG-MD simulations. The AA-MD and CG-MD simulations agree reasonably well with each other.

T (K)	End-to-End Distance (Å)		Radius of Gyration (Å)	
	AA-MD	CG-MD	AA-MD	CG-MD
300	38.6±0.1	57.0±0.3	15.2±0.1	19.5±0.1
500	38.3±0.2	46.1±0.7	15.2±0.1	17.1±0.1

As mentioned earlier, we chose two representative thermodynamic states in the MS-IBI process to derive the nonbonded potential: (i) T = 500 K (above the melting temperature) and ρ = 0.71 g/cm^3; and (ii) T = 300 K (room temperature) and ρ = 0.82 g/cm^3. **Supplementary Fig. 18(a, b)** shows the converged RDF after 7 iterations, where the averaged merit function f over the above two states equals to 0.015, satisfying the converge criterion. Due to the difference in the angle distribution between CG-MD and AA-MD simulations, it is challenging to perfectly match the RDF from CG-MD simulation with that from AA-MD simulation. To correct for the pressure difference between CG-MD simulations under the *NVT* ensemble with the target pressure of 1 bar, a linear correction term $\Delta V(r)$ is added to the numerical potential obtained from the last iteration[15]:

$$\Delta V(r) = V_0\left(1 - \frac{r}{r_{cutoff}}\right) \tag{S8}$$

where V_0 is the only parameter to adjust, which is positive or negative depending on whether the present pressure is lower or higher than the target pressure. $V_0 = 0.1\ k_bT$ is chose here as a typical adjusted amplitude.

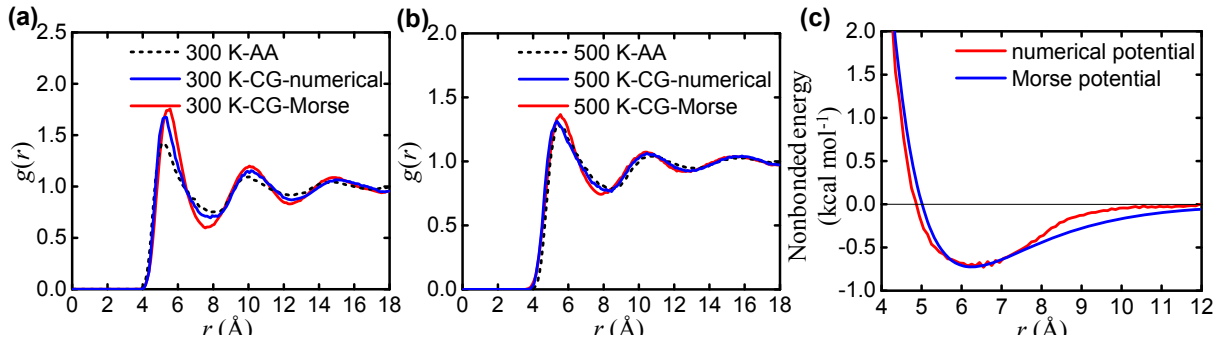

Supplementary Figure 18. The target RDF $g(r)$ from AA-MD simulations, and the final RDFs from CG-MD simulations using the numerical nonbonded potential directly obtained from MS-IBI and the fitted analytical Morse-style nonbonded potential at (a) 300 K and (b) 500 K. (c) Comparison between the optimized nonbonded pair-wise potential curve in the numerical form obtained directly from MS-IBI and that from the fitted analytical Morse-style nonbonded potential.

The optimized nonbonded potential curve (in the numerical form) is shown in **Supplementary Fig. 18(c)**. Considering the shape of the optimized nonbonded potential curve, an analytical Morse-style functional form is best suited to fit such a numerical nonbonded potential, as shown in **Supplementary Fig. 18(c)**. Specifically,

$$V_{nonbonded} = D_e\left[e^{-2\alpha_e(r-r_0)} - 2e^{-\alpha_e(r-r_0)}\right] \quad \text{(S9)}$$

where r_0 is the equilibrium bead distance, $-D_e$ is the minimum potential energy, and α_e measures the rate of decay of the potential. The resulting RDF $g(r)$ from CG-MD simulations using the Morse-style nonbonded potential is also shown in **Supplementary Fig. 18(a, b)** for comparison. Although the numerical nonbonded potential could be used in a tabulated form, we applied the analytical Morse nonbonded potential in all the work here to allow better transferability of the CG potential developed here. The final optimized CG potential parameters are listed in

Supplementary Table 2.

Supplementary Table 2: Final optimized CG potential parameters.

Interactions	CG Potential Parameters
Bond	l_0 = 5.8 Å, D_b = 84 kcal mol^{-1}, α_b = 0.44 Å^{-1}
Angular	k_a = 4 kcal mol^{-1}
Nonbonded	r_0 = 6.3 Å, D_e = 0.725 kcal mol^{-1}, α_e = 0.56 Å^{-1}

Finally, the glass transition temperature T_g (where polymers transit from the glassy to the rubbery state) and the melting temperature T_m are important characteristics of polymer materials, so they were used here to validate the CG potential. T_g was identified by the transition in the slope of the volume vs. temperature curve under the *NPT* ensemble (P = 1 bar)[16,17], as shown in **Supplementary Fig. 19(a).** Following the quenching procedure when preparing bulk PE samples, the sample at 300 K was further quenched to 100 K at the same cooling rate of 2 K ns^{-1}. The intersection of the two lines gives an estimate of T_g = 255 K, which is close to the experimentally-measured value of ~250 K[18] of bulk PE at a molecular weight of 1.4×10^5 g mol^{-1}. T_m was deduced by the hysteresis method as $T_m = T^+ + T^- - \sqrt{T^+T^-}$, where T^+ and T^- are the phase changing temperatures under superheating and supercooling conditions, respectively[19]. Specifically, T^+ = 517 K was determined by the location of the step in the density vs. temperature curve by heating a PE crystal consisting of 36 150-bead chains from 300 K to 700 K

at a rate of 2 K ns^{-1} (**Supplementary Fig. 19(b)**). T^- is hard to estimate due to the rare crystal nucleation event in the time-limited CG-MD simulations, and therefore, was approximated by $T^- \approx T_g$ [20]. As a result, T_m is estimated to be 409 K here, which is very close to the experimentally-measured value of 410 K [21] for bulk PE system at a molecular weight of 2×10^4 g mol^{-1}.

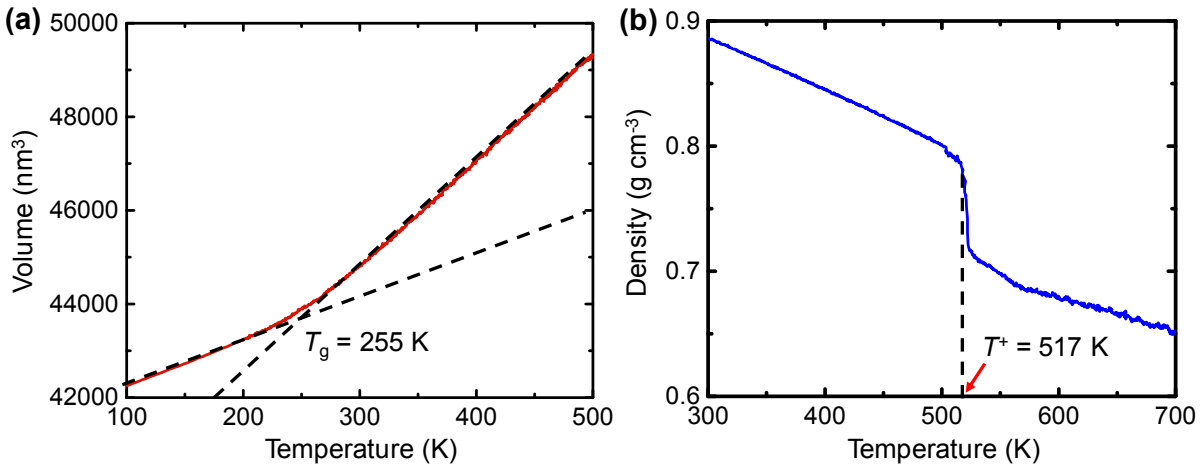

Supplementary Figure 19. (a) CG-MD simulated system volume evolution as a function of temperature, which was used to determine the glass transition temperature. (b) The density vs. temperature profile obtained through heating a PE crystal consisting of 36 150-bead chains, which was used to determine the superheating phase change temperature.

REFERENCES

1 Stukowski, A. Computational analysis methods in atomistic modeling of crystals. *JOM* **66**, 399-407, (2013).

2 Stukowski, A. Visualization and analysis of atomistic simulation data with OVITO–the open visualization tool. *Modelling and Simulation in Materials Science and Engineering* **18**, 015012, (2009).

3 Nguyen, H. T., Smith, T. B., Hoy, R. S. & Karayiannis, N. C. Effect of chain stiffness on the competition between crystallization and glass-formation in model unentangled polymers. *The Journal of Chemical Physics* **143**, 144901, (2015).

4 Stuart, S. J., Tutein, A. B. & Harrison, J. A. A reactive potential for hydrocarbons with intermolecular interactions. *The Journal of Chemical Physics* **112**, 6472-6486, (2000).

5 Shen, S., Henry, A., Tong, J., Zheng, R. & Chen, G. Polyethylene nanofibres with very high thermal conductivities. *Nature Nanotechnology* **5**, 251-255, (2010).

6 Shulumba, N., Hellman, O. & Minnich, A. J. Lattice thermal conductivity of polyethylene molecular crystals from first-principles including nuclear quantum effects. *Physical Review Letters* **119**, 185901, (2017).

7 Dee, G. T., Ougizawa, T. & Walsh, D. J. The pressure-volume-temperature properties of polyethylene, poly (dimethyl siloxane), poly (ethylene glycol) and poly (propylene glycol) as a function of molecular weight. *Polymer* **33**, 3462-3469, (1992).

8 Zhao, J., Nagao, S. & Zhang, Z. Thermomechanical properties dependence on chain length in bulk polyethylene: Coarse-grained molecular dynamics simulations. *Journal of Materials Research* **25**, 537-544, (2010).

9 Laso, M. & Perpete, E. A. *Multiscale Modelling of Polymer Properties*. 31-45 (Elsevier, 2006).

10 Nosé, S. A unified formulation of the constant temperature molecular dynamics methods. *The Journal of Chemical Physics* **81**, 511-519, (1984).

11 Hoover, W. G. Canonical dynamics: Equilibrium phase-space distributions. *Physical Review A* **31**, 1695, (1985).

12 Salerno, K. M., Agrawal, A., Perahia, D. & Grest, G. S. Resolving dynamic properties of polymers through coarse-grained computational studies. *Physical Review Letters* **116**, 058302, (2016).

13 Reith, D., Pütz, M. & Müller-Plathe, F. Deriving effective mesoscale potentials from atomistic simulations. *Journal of Computational Chemistry* **24**, 1624-1636, (2003).

14 Blanksby, S. J. & Ellison, G. B. Bond dissociation energies of organic molecules. *Accounts of Chemical Research* **36**, 255-263, (2003).

15 Milano, G. & Müller-Plathe, F. Mapping atomistic simulations to mesoscopic models: A systematic coarse-graining procedure for vinyl polymer chains. *The Journal of Physical Chemistry B* **109**, 18609-18619, (2005).

16 Han, J., Gee, R. H. & Boyd, R. H. Glass transition temperatures of polymers from molecular dynamics simulations. *Macromolecules* **27**, 7781-7784, (1994).

17 Hossain, D. *et al.* Molecular dynamics simulations of deformation mechanisms of amorphous polyethylene. *Polymer* **51**, 6071-6083, (2010).
18 Magill, J. H., Pollack, S. S. & Wyman, D. P. Glass temperature and crystal modification of linear polymethylene. *Journal of Polymer Science Part A: General Papers* **3**, 3781-3786, (1965).
19 Luo, S.-N., Strachan, A. & Swift, D. C. Nonequilibrium melting and crystallization of a model Lennard-Jones system. *The Journal of Chemical Physics* **120**, 11640-11649, (2004).
20 Zheng, L., Luo, S.-N. & Thompson, D. L. Molecular dynamics simulations of melting and the glass transition of nitromethane. *The Journal of Chemical Physics* **124**, 154504, (2006).
21 Gopalan, M. R. & Mandelkern, L. Effect of crystallization temperature and molecular weight on the melting temperature of linear polyethylene. *The Journal of Physical Chemistry* **71**, 3833-3841, (1967).